



Published in final edited form as:

Phys Biol. ; 18(1): 015001. doi:10.1088/1478-3975/abc5ad.

Liquid–liquid phase separation driven compartmentalization of reactive nucleoplasm

Rabia Laghmach^{1,2,3}, Davit A Potoyan^{1,2,3,*}

¹Department of Chemistry, Iowa State University, Ames, IA 50011, United States of America

²Department of Biochemistry, Biophysics and Molecular Biology, Iowa State University, Ames, IA 50011, United States of America

³Bioinformatics and Computational Biology program, Iowa State University, Ames, IA 50011, United States of America

Abstract

The nucleus of eukaryotic cells harbors active and out of equilibrium environments conducive to diverse gene regulatory processes. On a molecular scale, gene regulatory processes take place within hierarchically compartmentalized sub-nuclear bodies. While the impact of nuclear structure on gene regulation is widely appreciated, it has remained much less clear whether and how gene regulation is impacting nuclear order itself. Recently, the liquid–liquid phase separation emerged as a fundamental mechanism driving the formation of biomolecular condensates, including membrane-less organelles, chromatin territories, and transcriptional domains. The transience and environmental sensitivity of biomolecular condensation are strongly suggestive of kinetic gene-regulatory control of phase separation. To better understand kinetic aspects controlling biomolecular phase-separation, we have constructed a minimalist model of the reactive nucleoplasm. The model is based on the Cahn–Hilliard formulation of ternary protein–RNA–nucleoplasm components coupled to non-equilibrium and spatially dependent gene expression. We find a broad range of kinetic regimes through an extensive set of simulations where the interplay of phase separation and reactive timescales can generate heterogeneous multi-modal gene expression patterns. Furthermore, the significance of this finding is that heterogeneity of gene expression is linked directly with the heterogeneity of length-scales in phase-separated condensates.

Keywords

phase separation; gene regulation; nucleoplasm; liquid–liquid phase separation; eukaryotic nucleus; nonequilibrium

Original content from this work may be used under the terms of the [Creative Commons Attribution 4.0 licence](#).

*Author to whom any correspondence should be addressed. potoyan@iastate.edu.

Supplementary material for this article is available online

1. Introduction

Phase separation is a fundamental mechanism for the emergent order in an ordinary and biological matter [1, 2]. Recently, phase separation of biomolecules has also become a cornerstone physical mechanism for understanding the intracellular organization [2–4]. A wide range of membrane-less compartments are found to form through biomolecular phase separation, including nucleoli [5–7], stress granules [8–10], chromatin domains [11–13] and transcriptional centers [14, 15]. The primary components driving the intra-cellular phase separation are proteins and nucleic acids with multi-valent interaction centers [16, 17].

The stickers-and-spacers framework has emerged as a viable model explaining the existence of a broad class of sequence encoded driving forces of disordered proteins which serve as nucleating centers for biomolecular condensates [3, 18]. These newly appreciated abilities of proteins and nucleic acids for forming large-scale liquid bodies is offering fresh avenues for understanding mechanisms of the coordinated action of biomolecules in gene regulation and cellular organization that go beyond single-molecule action. It is well known that eukaryotic nuclei are rich in disordered proteins linked with transcription and chromatin architecture reorganization activities [19, 20]. There have been several proposals of the functional roles that may include catalysis of biochemical reactions, noise buffering and inducing ultra-sensitive signals [21–23]. However, understanding the mechanistic picture that links phase separation to the functional gene regulatory processes inside the nucleus has remained elusive [22] due to heterogeneous, multiscale, and non-equilibrium nature of the nuclear environment [24].

In this work, we propose a minimal model of a reactive nucleoplasm (figure 1) with an objective to illustrate, in a proof of principle manner; (i) how spatially resolved non-equilibrium reactive events generate qualitatively distinct from equilibrium phase behavior and (ii) how the interplay of various kinetic timescales in the system impacts gene expression patterns. The minimal reactive nucleoplasm model consists of a ternary solution filled with incompressible fluid consisting of ‘active’ protein, RNA components, and ‘passive’ nucleoplasmic buffer. The mathematical formulation of the model is based on a generic ternary diffuse interface model of one-step transcription/translation and phase-separation inside the nucleoplasm. The model resolves the formation and dissolution of protein–RNA droplets as well as reactive events of influx/creation and out-flux/degradation of proteins and RNA. By an extensive set of simulations exploring the interplay of timescales in the system, we found a broad kinetic regime dominated by length-scale heterogeneity of phase-separated droplets which correspond to heterogeneous gene expression patterns.

Various simple mathematical models have been used to explore generic aspects of equilibrium and non-equilibrium phase-separation as well as the physical properties of resulting condensates [25–33]. The most relevant to the present contribution are the work by Berry *et al* [29], Tang and Yang [33], and Glotzer [32], where authors have considered a binary and ternary fluid model of nucleoplasm, which couples phase separation with first-order exchange among soluble and insoluble components. Authors have simulated different stages of spinodal decomposition and explored its impact on Ostwald ripening of droplets. It

was shown that kinetics of the RNA flux accelerates the ripening of droplets, thereby showing a link between the thermodynamics of phase separation and kinetics of droplet formation. Other recent notable studies worth highlighting here include the work by Yamamoto *et al* [30], which have studied the non-spatial model of architectural RNA phase separation coupled with non-equilibrium production. Finally, an important theoretical framework by Ilker and Joanny [34] establishes an equivalence of phase-separation kinetics with the Cahn–Hilliard effective temperature.

Some of the key distinctions of the present model from previous studies include (i) spatially resolved formulation of gene expression and phase separation (ii) explicit connection of phase-separated patterns with transcription and translation models of gene expression (iii) exploring the impact of dynamic turnover in RNA–protein–nucleoplasm ternary diagram on global patterning. Thus, the present work clarifies as a first step the dual nature of nuclear order and gene expression, and provides a useful theoretical framework for understanding equilibrium and non-equilibrium origins of intra-nuclear patterning.

2. Minimal reactive nucleoplasm model

In order to explore the kinetics of phase separation of RNA–proteins–nucleoplasm reacting mixture, we use a local thermodynamic approach that describes the phase separation of a ternary mixture based on the Flory–Huggins model [35, 36] for polymer solutions coupled with chemical reaction-diffusion equations (figure 1). In this section, we describe the mathematical formulation of the model of a ‘minimal reactive nucleoplasm’: where the liquid–liquid phase separation of single RNA and protein components is coupled with reactive events of transcription, translation, and degradation.

A minimal one-step model of independent, unregulated transcription and translation [37] is used to set the lifetimes of protein and RNA components comprising the nucleoplasmic milieu defined by the following chemical reactions:



where the k_R , k_P and k_d are the rate coefficients for transcription, translation and degradation, respectively; The \emptyset symbol is used to denote the degradation of RNA and protein. The kinetics of phase separation of ternary reactive protein–RNA–nucleoplasm mixture is given by the following set of reaction–diffusion equations [32]:

$$\frac{\partial \varphi_1}{\partial t} = \nabla \left(M_1(\{\varphi_i\}) \nabla \left(\frac{\partial F[\{\varphi_i\}]}{\partial \varphi_1} \right) \right) + f_1(r) [k_R(1 - \varphi_1 - \varphi_2) - k_d \varphi_1] \quad (2)$$

$$\frac{\partial \varphi_2}{\partial t} = \nabla \left(M_2(\{\varphi_i\}) \nabla \left(\frac{\partial F[\{\varphi_i\}]}{\partial \varphi_2} \right) \right) + f_2(r) [k_P(1 - \varphi_1 - \varphi_2) - k_d \varphi_2], \quad (3)$$

where $\varphi_i (i = 1, 2, 3)$ are the order parameter variables associated with the local concentration of i th-component forming the mixture, M_i are their corresponding mobility coefficients, and F is the free energy functional describing the thermodynamics of ternary mixture. The total local density in the system is considered constant, respecting the incompressibility condition expressed as: $\sum_{i=1}^3 \varphi_i = 1$. The indices 1, 2, and 3 denote RNA, protein, and nucleoplasm, respectively. The function $f_1(r)$ and $f_2(r)$ are used to define the spatially heterogeneous distribution of components mimicking RNA expression inside nucleus and protein translation and flow into nucleus. The RNA is created in the center of nucleoplasm thereby mimicking a transcriptional process [38], herein we used the function defined as $f_1(r) = \exp(-(r - r_c)^2/a)$ where r is the distance from the center of the domain located at r_c . The coefficient a is a localization lengthscale which is set to $a = 1$. The protein component is flown into the nucleus from the nuclear boundaries thereby mimicking translation [38], herein we used the function defined as $f_2(r) = 1$ on the domain boundary Ω and 0 otherwise. Heterogeneous mobility is an interesting aspect of nucleoplasm [39], however, and is undoubtedly deserving of a separate investigation. For simplicity, we assume the mobility coefficients for all components to be constant $M_1(\{\varphi_i\}) = M_2(\{\varphi_i\}) = M$. The free energy functional taken in this model is based on the Flory–Huggins energy formulation of the ternary mixture system [40, 41], which is given by:

$$F[\{\varphi_i\}] = \int d\Omega \left[f_{\text{bulk}}(\varphi_1, \varphi_2, \varphi_3) + \sum_i \frac{\kappa_{\varphi_i}}{2} |\nabla \varphi_i|^2 \right] \quad (4)$$

with

$$f_{\text{bulk}}(\varphi_1, \varphi_2, \varphi_3) = \sum_i \frac{\varphi_i}{N_i} \ln(\varphi_i) + \sum_{i \neq j} \chi_{ij} \varphi_i \varphi_j.$$

where $f_{\text{bulk}}(\varphi_1, \varphi_2, \varphi_3)$ is the local free energy density, and the square-gradient coefficients κ_{φ_i} are positive constants controlling the interfacial free energies. χ_{ij} are the interaction parameters between species i - j , and N_i is the degree of polymerization.

We note here that there also exist other mathematical formulations of the local free energy for describing the phase separation of ternary polymeric mixtures. For instance, the generalized multiwell potential used by Yang *et al* [42] to study multiphase systems where the local free energy density is the summation of all the double-well potential for each phase-field variable complemented by a polynomial term that connects all the variables altogether.

The dynamic equations are brought to a dimensionless form, which reveals the essential time- and length-scales of the problem. Let us introduce l , the characteristic length of the system, and τ is the characteristic time. The dimensionless form of the kinetic equations yields four dimensionless parameters that control the dynamics of phase-separation where components are undergoing chemical reactions. The $\tau_D/\tau = l^2(M \times \tau) = 1$ is the ratio between diffusion timescale and characteristic time which is fixed to be a unit. The $\tau/\tau_T = \tau \times k_T$ is the ratio between characteristic time and time-scale associated with transcription.

The $\tau/\tau_p = \tau \times k_p$ is the ratio between characteristic time and time-scale associated with protein formation. The $\tau/\tau_d = \tau \times k_d$ is ratio between characteristic time and time-scale associated with degradation. To solve the dynamic equations (2) and (3) in the dimensionless form, we use a fully implicit finite element C++ library from the multiphysics object-oriented simulation environment (MOOSE) [43]. The simulations were performed on a rectangular domain of dimensions $L_x \times L_y : (50 \times 50)$, with periodic boundary conditions. A quadrilateral element QUAD4 with four nodes was used for domain meshing with the refinement. The total number of elements used for the fine mesh is 10 000. The time step of integration Δt is fixed at 0.05 (a.u.). In this work, we only consider the case of a symmetric ternary mixture undergoing a chemical reaction with $\chi_{12} = \chi_{23} = \chi_{13} = 3$ that ensures phase-separation of protein–RNA droplets in the absence of chemical reactions $\chi > \chi_c$, where χ_c denote the critical point. We also assumed that the chemical reaction takes place at the comparable scales with the phase separation process. Near the critical point χ_c , the mean-field Flory–Huggins free energy can be approximated through Taylor expansion via Landau form [32]. It is important to construct representative free energy functional that accounts for fluctuations of the phase-field variables that are dominant near the critical point. To express the critical behavior a new formulation of the free energy of mixing renormalized by the spatial variation has been proposed by Yamamoto *et al* [44, 45]. The chain lengths N_i , or degree of polymerization, are assumed to be the same: $N_1 = N_2 = N_3 = 1$. It is noted here that the entropic term of the local free energy is proportional to the inverse polymeric lengths N_i . As a consequence of the reduction of entropy for long-chain lengths, the phase diagrams and the spinodal curve will be modified in the way to increase the separating-phase region of the phase diagram. In this case, a small variation of the interaction parameter between species will lead easily to phase separation. The impact of phase-separation of small and large chains such as genomic regions and proteins/RNA could be an interesting study to address in future investigations. The other parameters of simulations were set to $\kappa_{\varnothing 1} = \kappa_{\varnothing 2} = 0.03125$. The initial configuration of phase-field variables is generated by $\varphi_i(x) = \langle \varphi_i \rangle + \delta\varphi_i$, where $\langle \varphi_i \rangle$ is an initial average concentration associated with φ_i , and $\delta\varphi_i$ is a small random perturbation amplitude. For all simulations presented here, the initial average of species i are set to $\langle \varphi_1 \rangle = 0.3$ and $\langle \varphi_2 \rangle = 0.09$, with $\delta\varphi_1 \in [-0.05, 0.05]$ and $\delta\varphi_2 \in [-0.01, 0.01]$.

3. Results

Here we report the findings obtained by analyzing the results of simulations with a minimal reactive nucleoplasm model. We have organized the results in three broad kinetic regimes, which are described by three orders of magnitude in degradation time-scale $\tau_d = \tau, 10\tau, 100\tau$ with respect to the diffusion time-scale τ . These time-scales correspond to different rates of turnover of nucleoplasmic components from fast to slow. For each regime, we have carried out extensive grid-based kinetic parameter sweeps exploring the coupling of transcriptional and transnational time-scales on the backdrop of fixed phase-separating free energy landscape of RNA–protein–nucleoplasm components. Despite the incredible simplicity of the minimal reactive nucleoplasm model, the time course of simulations (figures 2–4) has revealed a non-trivial patterning of nucleoplasm which are a dramatic

departure from equilibrium thermodynamics of ternary phase separation in the absence of spatially non-uniform reaction–diffusion.

We start by investigating the fast dynamical regime corresponding to $\tau_d = \tau$. Figure 2 shows the spatial and temporal evolution of RNA–protein components in a reactive nucleoplasm environment. Four interesting cases are highlighted in figure 2, corresponding to different time-scale separation between translation τ_P and transcription τ_R processes. When $\tau_P = \tau_R = \tau$ we observe rapid coarsening dynamics (droplet growth kinetics) and emergence of RNA droplets with stable ‘protein front’ by which we refer to the formation of protein layer surrounding nucleoplasm domain edges [figure 2(A)]. Coarsening dynamics for either protein front or RNA droplets are also observed for fast translation/slow transcription or slow translation/fast transcription, respectively [figures 2(B) and (C)]. Naturally, it is expected that the more rapid degradation timescales for RNA and protein lead to the disappearance of both RNA droplets and protein fronts [figure 2(D)]. Thus, we can conclude that in the fast dynamical regime, nucleoplasm patterns are entirely set by the kinetic parameters with thermodynamic free energy landscape taking the back seat.

The formation of RNA–protein patterns is more intricate in the intermediate dynamical regime corresponding to $\tau_d = 10\tau$ (figure 3). In the figure 3, we show the patterns arising from competing transcription, translation, and degradation with different transcription and translation timescales. When both transcription and translation have comparable time scales [figure 3(A)] to that of diffusion, we find a rapid progression of protein front on the one hand and a rapid RNA seed droplet growth at on the other. In this regime, once the nucleoplasm reaches a non-equilibrium steady state, droplet patterning is now becomes dictated by the thermodynamics of Flory–Huggins interaction parameters, which set the extend of mixing between protein and RNA components. When both the transcription and translation have the same time scale but are now significantly slower than diffusion [figure 3(D)], then the system displays heterogeneity in protein RNA droplet distribution. The situation with faster transcription and the faster translation is predictable: [figures 3(B) and (C)] the system tends to increase in protein front and RNA nucleating center, respectively. We have only highlighted the most interesting cases for each dynamical regime. The simulation results for the full set of time-scales are presented in the supporting information (<https://stacks.iop.org/PB/18/015001/mmedia>) figure S1–S10. The tempo ral evolution of average concentration for different kinetic regimes with $\tau_R = \tau_P = 100\tau$ is shown in figure S14.

We now turn to the analysis of the slow dynamical regime corresponding to a degradation timescale $\tau_d = 100\tau$. In this regime, we once again high-light four interesting cases [figures 4(A)–(D)]. When the system has comparable timescales for transcription, translation, and diffusion $\tau_P = \tau_R = \tau$, the nucleoplasmic component gets eliminated, and the system rapidly reaches a balance between protein front and RNA seed. Slowing down the translation $\tau_P = 100\tau_R = 100\tau$ by two orders of magnitude leads to a non-trivial patterning with the RNA seed, nucleoplasm and RNA droplets all con-existing at a non-equilibrium steady-state. On the other hand, slowing down the transcription [figure 4(C)] leads to a steady-state with significantly downsized RNA-seed at the expense of the peripheral protein front. Slowing down both transcription and translation [figure 4(D)] leads to a non-trivial patterning with

protein front, RNA droplets, and nucleoplasmic environment, but this time with no dominant RNA-seed.

To quantify the emergence of different droplet patterns, we have summarized the phase behavior of a reactive nucleoplasm model via. Global kinetic phase diagram, figure 5. Here one can see a global picture of how the interplay of kinetic timescales is favoring uniform vs binary vs ternary phases.

In order to quantify the length-scales of emergent patterns, we have analyzed the azimuthally averaged dynamic structure factors $S(k, t) = \int d\mathbf{k}_Q S(\mathbf{k}, t)$ associated with each dynamical regime (see figure 6 and supporting information, figure S11–S13). Analyzing dynamic structure factors reveals characteristic length-scales of protein/RNA droplets as well as emergent dynamical heterogeneity manifesting in the fast or slow coarsening of the droplets. The computed structure factors show a broad range of kinetically controlled states where one has bi-modality of RNA (or protein) components. This bimodality or more broadly heterogeneity of distribution is directly linked to the heterogeneity of droplet sizes and shapes that one can quantify from simulation images (figures 3 and 4). Multi-modal gene expression is a feature often linked with phenotypic heterogeneity and which has been mostly explained by citing the underlying non-linear dynamics of dichotomous switching noise in a spatially uniform master equation formalism [46–48]. The results of figure 6 clearly show that transcriptional heterogeneity can originate purely from the spatially non-uniform nature of gene expression, which is being modulated by timescales of phase separation, transcription, and translation.

Finally, we have computed the length scale of patterns summarizing transitional heterogeneity in three kinetic regimes of the minimal reactive nucleoplasm model (figure 7). The length-scales patterns are quantified by using pre-computed azimuthally averaged

dynamic structure factors $R(t) = \frac{\int dk S(k, t) k^{-2}}{\int dk S(k, t) k^{-1}}$ [49]. The length-scale patterns $R(t)$ quantify

the dominant length-scales which emerge during the time-evolution of a reactive nucleoplasm. Analyzing the evolution of length-scale patterns for three dynamical regimes, we see clearly that for the fast dynamical regime, there is only one dominating length-scale, which is dictated by the rapid degradation kinetic timescale. For the intermediate and slow dynamical regimes, however, we find heterogeneity of length-scales, which emerges from the disparity in transcription and translational timescales. We note that this heterogeneity has both structural and dynamical manifestations, as one can see by analyzing the power law of length-scale patterns $R(t) \sim At^\alpha$. We find two exponents, one which is characteristic for the early coarsening stage ($\alpha \sim 1/3$) and second ($\alpha \sim 3/8$) for the later accelerated phase separating evolution toward a steady state. We note that power laws in the dynamical variables of the nucleoplasmic environment have been detected and characterized in a large number of experiments [39, 50]. These power-law dependencies, however, are hard to disentangle in terms of distinct contributions since their origin may come from any combination of phase-separation, polymeric effects, confinement, and non-equilibrium motorized activities in the nucleus. In this work, we have only managed to scratch at the surface of the fascinating dynamical patterning potential of the active nucleoplasmic environment. For future studies, it would be interesting to investigate the impact of

differential mobility, hydro-dynamical coupling, and as well as investigate gene expression beyond a simple one-step model of unregulated reactions that have not been done in the present contribution.

4. Conclusion

Recent *in vitro* experiments with binary and ternary protein and RNA mixtures [51–53] have shown the rich complexity of phases which can emerge through liquid–liquid phase separation via modulation of stoichiometry of components and point mutations. These experiments show potentially novel regulatory strategies which when combined with non-equilibrium cellular processes such as transcription and translation could produce coordinated gene regulatory and signaling actions.

To this end, in the present contribution we introduce a minimal reactive nucleoplasm model combining spatially dependent transcription and translation to liquid–liquid phase separation of RNA and protein components embedded in the back-drop of passive nucleoplasm buffer. We use the minimal reactive-nucleoplasm model to cleanly dissect how the interplay of transcription, translation, and degradation time scales couples with the liquid–liquid phase separation of RNA and protein components in a model ternary solution. By carrying out extensive grid-based sweeps of kinetic parameter space, we uncover various non-trivial patterning and length-scale heterogeneity compared to the classic Flory–Huggins thermodynamic picture for ternary polymeric solutions. Our central finding is the existence of a broad kinetic regime characterized by a slow turnover of components and timescale disparity between transcription and translation under which a phase separating system can display bi-modal distribution. The significance of this finding is that the observed heterogeneity of gene expression is linked directly with the heterogeneity of length-scales in phase-separated condensates. The main findings and the minimal reactive nucleoplasm model thus establishes a useful framework with which one can further elucidate the emergence of nucleoplasm patterns and phenotype heterogeneity from first principles modeling of phase-separation and reaction–diffusion processes.

Supplementary Material

Refer to Web version on PubMed Central for supplementary material.

Acknowledgments

Research reported in this publication was supported by the National Institute of General Medical Sciences of the National Institutes of Health under Award No. R35GM138243. The content is solely the responsibility of the authors and does not necessarily represent the official views of the National Institutes of Health. This work used the Extreme Science and Engineering Discovery Environment (XSEDE), which is supported by the National Science Foundation Grant No. ACI-1548562 [54] on the Stampede2 machine at the Texas Advanced Computing Center (TACC) through allocation CTS190023. The authors acknowledge the Texas Advanced Computing Center (TACC) at The University of Texas at Austin for providing HPC resources that have contributed to the research results reported within this paper. The authors also acknowledge financial support from Iowa State University.

References

- [1]. Muñoz MA. 2018; Colloquium: criticality and dynamical scaling in living systems. *Rev. Mod. Phys.* 90:031001.

- [2]. Berry J, Brangwynne CP and Haataja M 2018 Physical principles of intracellular organization via active and passive phase transitions *Rep. Prog. Phys* 81 046601 [PubMed: 29313527]
- [3]. Choi J-M, Holehouse AS and Pappu RV 2020 Physical principles underlying the complex biology of intracellular phase transitions *Annu. Rev. Biophys* 49 107–33 [PubMed: 32004090]
- [4]. Dignon GL, Best RB and Mittal J 2020 Biomolecular phase separation: from molecular driving forces to macroscopic properties *Annu. Rev. Phys. Chem* 71 53–75 [PubMed: 32312191]
- [5]. Latonen L. 2019; Phase-to-Phase with nucleoli—stress responses, protein aggregation and novel roles of RNA. *Front. Cell. Neurosci.* 13:151. [PubMed: 31080406]
- [6]. Frottin F et al. 2019 The nucleolus functions as a phase-separated protein quality control compartment *Science* 365 342–7 [PubMed: 31296649]
- [7]. Feric M, Vaidya N, Harmon TS, Mitrea DM, Zhu L, Richardson TM, Kriwacki RW, Pappu R V and Brangwynne C P 2016 Coexisting liquid phases underlie nucleolar subcompartments *Cell* 165 1686–97 [PubMed: 27212236]
- [8]. Van Treeck B, Protter DSW, Matheny T, Khong A, Link CD and Parker R 2018 RNA self-assembly contributes to stress granule formation and defining the stress granule transcriptome *Proc. Natl Acad. Sci. USA* 115 2734–9 [PubMed: 29483269]
- [9]. Molliex A, Temirov J, Lee J, Coughlin M, Kanagaraj AP, Kim HJ, Mittag T and Taylor JP 2015 Phase separation by low complexity domains promotes stress granule assembly and drives pathological fibrillization *Cell* 163 123–33 [PubMed: 26406374]
- [10]. Riback JA, Katanski CD, Kear-Scott JL, Pilipenko EV, Rojek AE, Sosnick TR and Drummond DA 2017 Stress-triggered phase separation is an adaptive, evolutionarily tuned response *Cell* 168 1028–40 [PubMed: 28283059]
- [11]. Zhang Y and Kutateladze TG 2019 Liquid–liquid phase separation is an intrinsic physicochemical property of chromatin *Nat. Struct. Mol. Biol* 25 1085–6
- [12]. Palikyras S and Papanonis A 2019 Modes of phase separation affecting chromatin regulation *Open Biol* 9 190167 [PubMed: 31615334]
- [13]. Laghmach R, Di Pierro M and Potoyan DA 2019 Mesoscale liquid model of chromatin recapitulates nuclear order of eukaryotes *Biophys. J* 118 2130–40 [PubMed: 31623887]
- [14]. Hnisz D, Shrinivas K, Young RA, Chakraborty AK and Sharp PA 2017 A phase separation model for transcriptional control *Cell* 169 13–23 [PubMed: 28340338]
- [15]. Boija A et al. 2018 Transcription factors activate genes through the phase-separation capacity of their activation domains *Cell* 175 1842–55 [PubMed: 30449618]
- [16]. Boeynaems S et al. 2018 Protein phase separation: a new phase in cell biology *Trends Cell Biol* 28 420–35 [PubMed: 29602697]
- [17]. Rhine K, Vidaurre V and Myong S 2020 RNA droplets *Annu. Rev. Biophys* 49 247–65 [PubMed: 32040349]
- [18]. Schuster BS et al. 2020 Identifying sequence perturbations to an intrinsically disordered protein that determine its phase-separation behavior *Proc. Natl Acad. Sci. USA* 117 11421–31 [PubMed: 32393642]
- [19]. Sawyer IA, Bartek J and Dundr M 2018 Phase separated microenvironments inside the cell nucleus are linked to disease and regulate epigenetic state, transcription and RNA processing *Semin. Cell Dev. Biol* 90 94–103 [PubMed: 30017905]
- [20]. Uversky VN. 2019; Intrinsically disordered proteins and their ‘mysterious’ (meta) physics. *Front. Phys.* 7
- [21]. Klosin A, Oltch F, Harmon T, Honigmann A, Jülicher F, Hyman AA and Zechner C 2020 Phase separation provides a mechanism to reduce noise in cells *Science* 367 464–8 [PubMed: 31974256]
- [22]. Stroberg W and Schnell S 2018 Do cellular condensates accelerate biochemical reactions? Lessons from microdroplet chemistry *Biophys. J* 115 3–8 [PubMed: 29972809]
- [23]. Wang Z, Potoyan DA and Wolynes PG 2018 Stochastic resonances in a distributed genetic broadcasting system: the NF κ B/I κ B paradigm *J. R. Soc. Interface* 15 20170809 [PubMed: 29343631]

- [24]. Peng A and Weber SC 2019 Evidence for and against liquid-liquid phase separation in the nucleus Non-coding RNA 5 50
- [25]. Wurtz JD and Lee CF 2018 Chemical-reaction-controlled phase separated drops: formation, size selection, and coarsening Phys. Rev. Lett 120 078102 [PubMed: 29542937]
- [26]. Pytowski L, Lee CF, Foley AC, Vaux DJ and Jean L 2020 Liquid-liquid phase separation of type II diabetes-associated IAPP initiates hydrogelation and aggregation Proc. Natl Acad. Sci. USA 117 12050–61 [PubMed: 32414928]
- [27]. Lee CF, Brangwynne CP, Gharakhani J, Hyman AA and Jülicher F 2013 Spatial organization of the cell cytoplasm by position-dependent phase separation Phys. Rev. Lett 111 088101 [PubMed: 24010479]
- [28]. Zwicker D, Seyboldt R, Weber CA, Hyman AA and Jülicher F 2017 Growth and division of active droplets provides a model for protocells Nat. Phys 13 408–13
- [29]. Berry J, Weber SC, Vaidya N, Haataja M and Brangwynne CP 2015 Rna transcription modulates phase transition-driven nuclear body assembly Proc. Natl Acad. Sci. USA 112 E5237–45 [PubMed: 26351690]
- [30]. Yamamoto T, Yamazaki T and Hirose T 2020 Phase separation driven by production of architectural RNA transcripts Soft Matter 16 4692–8 [PubMed: 32396591]
- [31]. Gasior K, Zhao J, McLaughlin G, Forest MG, Gladfelter AS and Newby J 2019 Partial demixing of RNA–protein complexes leads to intradroplet patterning in phase-separated biological condensates Phys. Rev. E 99 012411 [PubMed: 30780260]
- [32]. Glotzer SC 1995 Computer simulations of spinodal decomposition in polymer blends Annu. Rev. Comput. Phys 2 1–46
- [33]. Tong C and Yang Y 2002 Phase-separation dynamics of a ternary mixture coupled with reversible chemical reaction J. Chem. Phys 116 1519–29
- [34]. Ilker E and Joanny J-F 2020 Phase separation and nucleation in mixtures of particles with different temperatures Phys. Rev. Res 2 023200
- [35]. Brangwynne CP, Tompa P and Pappu RV 2015 Polymer physics of intracellular phase transitions Nat. Phys 11 899–904
- [36]. Flory PJ 1942 Thermodynamics of high polymer solutions J. Chem. Phys 10 51–61
- [37]. Kepler TB and Elston TC 2001 Stochasticity in transcriptional regulation: origins, consequences, and mathematical representations Biophys. J 81 3116–36 [PubMed: 11720979]
- [38]. Alberts B. 2018 Molecular Biology of the Cell.
- [39]. Caragine CM, Haley SC and Zidovska A 2019 Nucleolar dynamics and interactions with nucleoplasm in living cells Elife 8 e47533 [PubMed: 31769409]
- [40]. Hohenberg PC and Halperin BI 1977 Theory of dynamic critical phenomena Rev. Mod. Phys 49 435
- [41]. Cahn JW and Hilliard JE 1958 Free energy of a nonuniform system. I. Interfacial free energy J. Chem. Phys 28 258–67
- [42]. Yang X, Zhao J, Wang Q and Shen J 2017 Numerical approximations for a three-component Cahn–Hilliard phase-field model based on the invariant energy quadratization method Math. Models Methods Appl. Sci 27 1993–2030
- [43]. Permann CJ. et al. 2020; MOOSE: enabling massively parallel multiphysics simulation. SoftwareX. 11:100430.
- [44]. Narita T, Yamamoto T, Hosoya E and Dobashi T 2003 Gibbs free energy expression for the system polystyrene in methylcyclohexane and its application to microencapsulation Langmuir 19 5240–5
- [45]. Yamamoto T, Narita T, Nobe M and Dobashi T 2004 Free energy of mixing for polymer solutions Macromolecules 37 3475–86
- [46]. Lin YT, Hufton PG, Lee EJ and Potoyan DA 2018 A stochastic and dynamical view of pluripotency in mouse embryonic stem cells PloS Comput. Biol 14 e1006000 [PubMed: 29451874]
- [47]. Hufton PG, Lin YT, Galla T and McKane AJ 2016 Intrinsic noise in systems with switching environments Phys. Rev. E 93 052119 [PubMed: 27300842]

- [48]. Potoyan DA and Wolynes PG 2015 Dichotomous noise models of gene switches J. Chem. Phys 143 195101 [PubMed: 26590554]
- [49]. Kendon VM, Cates ME, Desplat J, Pagonabarraga I and Bladon P 2000 Inertial effects in three dimensional spinodal decomposition of a symmetric binary fluid mixture: a lattice Boltzmann study (arXiv:cond-mat/0006026)
- [50]. Zidovska A 2020 The self-stirred genome: large-scale chromatin dynamics, its biophysical origins and implications Curr. Opin. Genet. Dev 61 83–90 [PubMed: 32497955]
- [51]. Alshareedah I, Moosa MM, Raju M, Potoyan DA and Banerjee PR 2020 Phase transition of RNA–protein complexes into ordered hollow condensates Proc. Natl Acad. Sci. USA 117 15650–8 [PubMed: 32571937]
- [52]. Kaur T, Raju M, Alshareedah I, Davis RB, Potoyan DA and Banerjee PR 2020 Sequence-encoded and composition-dependent protein–RNA interactions control multiphasic condensate topologies (10.1101/2020.08.30.273748)
- [53]. Lu T and Spruijt E 2020 Multiphase complex coacervate droplets J. Am. Chem. Soc 142 2905–14 [PubMed: 31958956]
- [54]. Towns J et al. 2014 Xsede: accelerating scientific discovery Comput. Sci. Eng 16 62–74

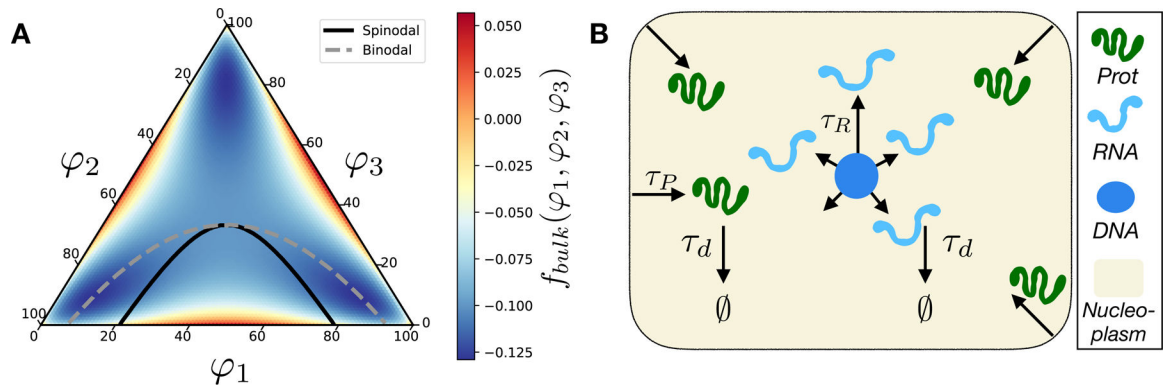


Figure 1.

(A) Phase diagram of the symmetric ternary protein–RNA–nucleoplasm mixture and the bulk free energy governing the solution thermodynamics $f_{\text{bulk}}(\varphi_1, \varphi_2, \varphi_3)$ for $\chi = 3$. The solid-line and dash-line correspond to the spinodal and binodal curves, respectively. (B) The schematic of the minimal reactive nucleoplasm model. Shown are the main reactive components (protein, RNA, DNA-seed, nucleoplasm reservoir), the corresponding reactive processes involving each components as well as their spatial generation profiles.

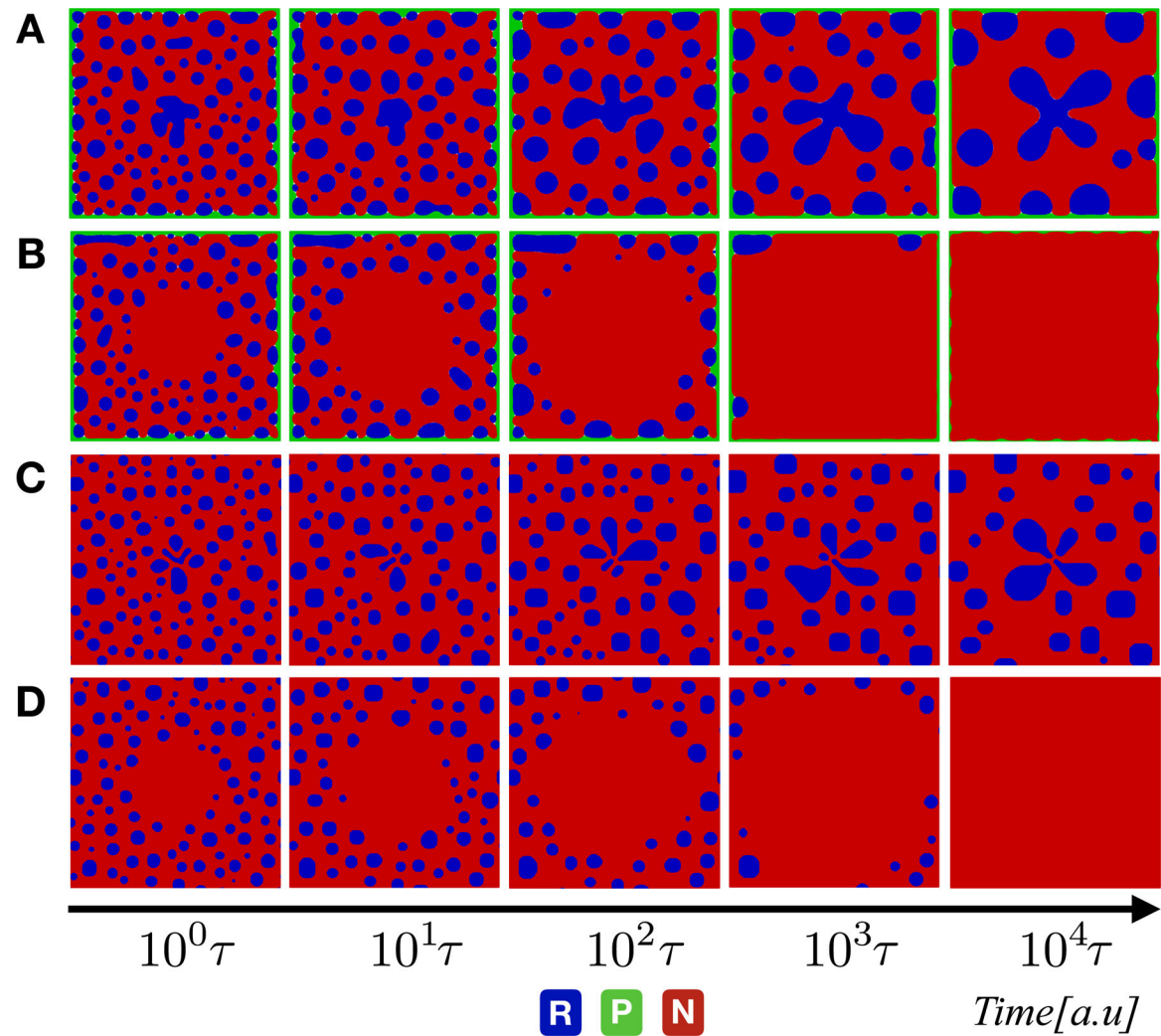


Figure 2.

Evolution of phase-field variables φ_i for three phase mixture undergoing the chemical reaction with a degradation time-scale fixed at the same of diffusion ($\tau_d = \tau$). From up to bottom: snapshots corresponding to simulation results with (A) $\tau_R = \tau_P = \tau$, (B) $\tau_R = 100\tau_P = 100\tau$, (C) $\tau_P = 100\tau_R = 100\tau$; and (D) $\tau_R = \tau_P = 100\tau$. The color code in blue, green, and red indicates the RNA, protein, and nucleoplasm regions, respectively.

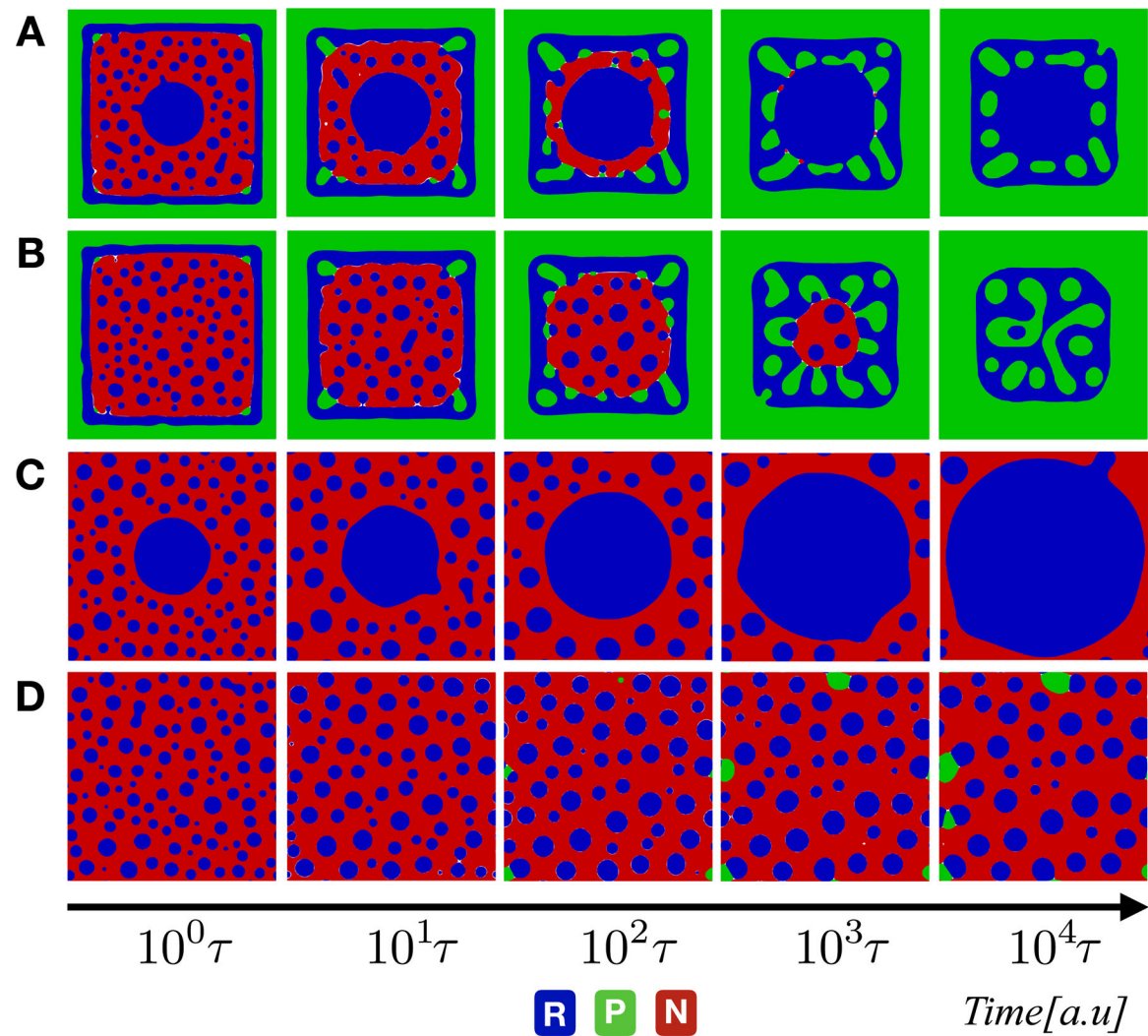


Figure 3.

Evolution of phase-field variables ϕ_i for three phase mixture undergoing the chemical reaction with a degradation time-scale fixed at the same of diffusion ($\tau_d = 10\tau$). From up to bottom: snapshots corresponding to simulation results with (A) $\tau_R = \tau_P = \tau$; (B) $\tau_R = 50\tau_P = 50\tau$; (C) $\tau_P = 100\tau_R = 100\tau$; and (D) $\tau_R = \tau_P = 50\tau$. The color code in blue, green, and red indicates the RNA, protein, and nucleoplasm regions, respectively.

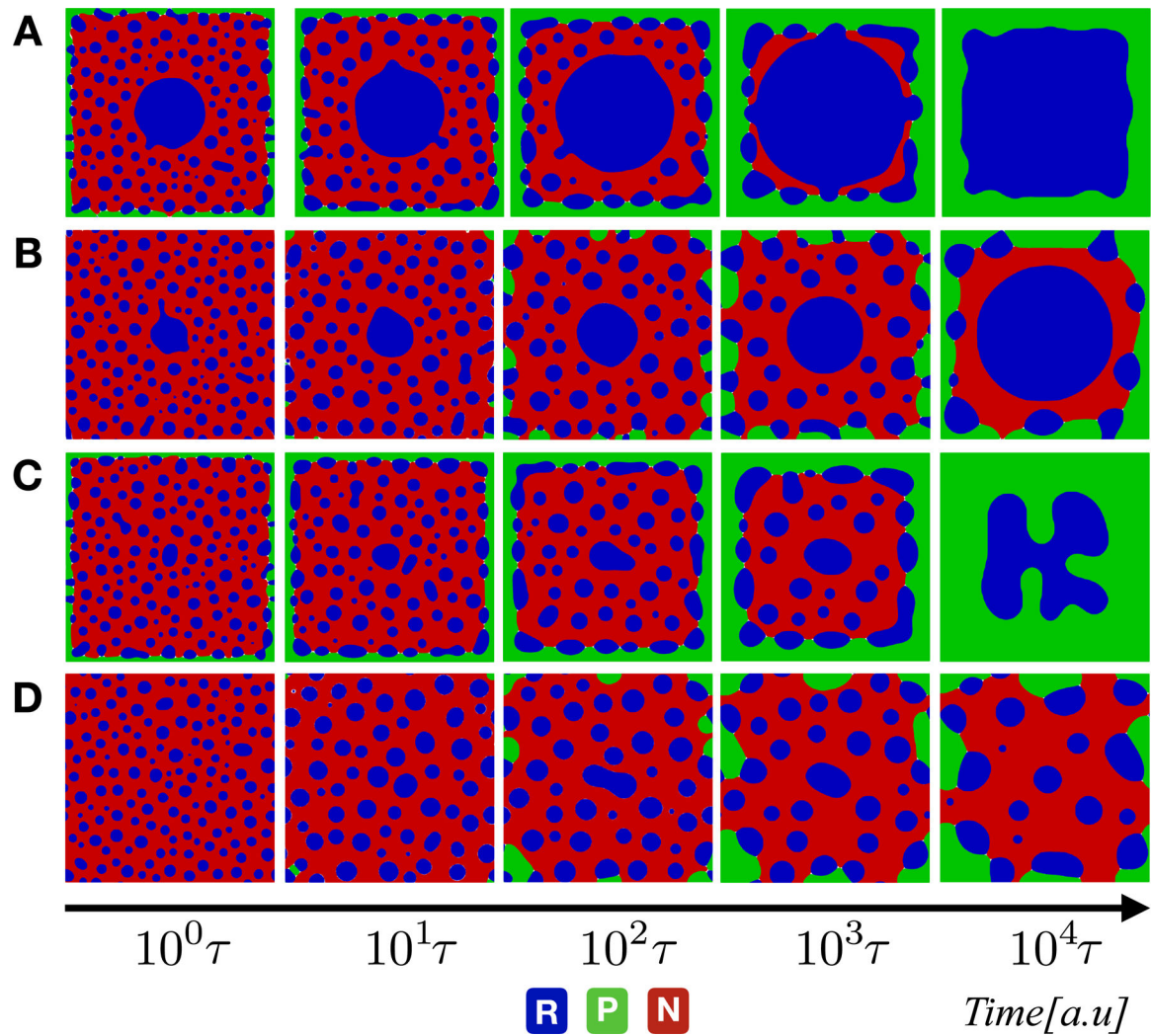


Figure 4.

Evolution of phase-field variables ϕ_i for three phase mixture undergoing the chemical reaction with a degradation time-scale fixed at the same of diffusion ($\tau_d = 100 \tau$). From up to bottom: snapshots corresponding to simulation results with (A) $\tau_P = 10 \tau_R = 10 \tau$, (B) $\tau_R = 10 \tau_P = 50 \tau$, (C) $\tau_R = 50 \tau_P = 10 \tau$, and (D) $\tau_R = \tau_P = 100 \tau$. The color code in blue, green, and red indicates the RNA, protein, and nucleoplasm regions, respectively.

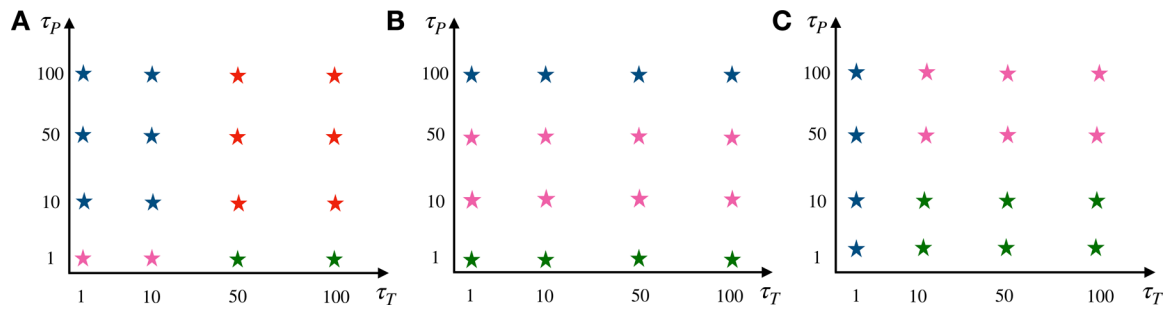


Figure 5.

Phase diagram: phase diagram showing the dominant steady-state phase and summarizing various patterns that arise at three kinetic regimes (A) $\tau_d = \tau$, (B) $\tau_d = 10\tau$, (C) $\tau_d = 100\tau$. The blue star indicates that the RNA domain becomes the dominant phase in the long timescale limit. The green star means that the proteins-droplets become the dominant phase in the long timescale limit. The pink star indicates three coexisting phases of the ternary mixture. In contrast, the red star indicates that RNA–proteins turn totally into the nucleoplasm.

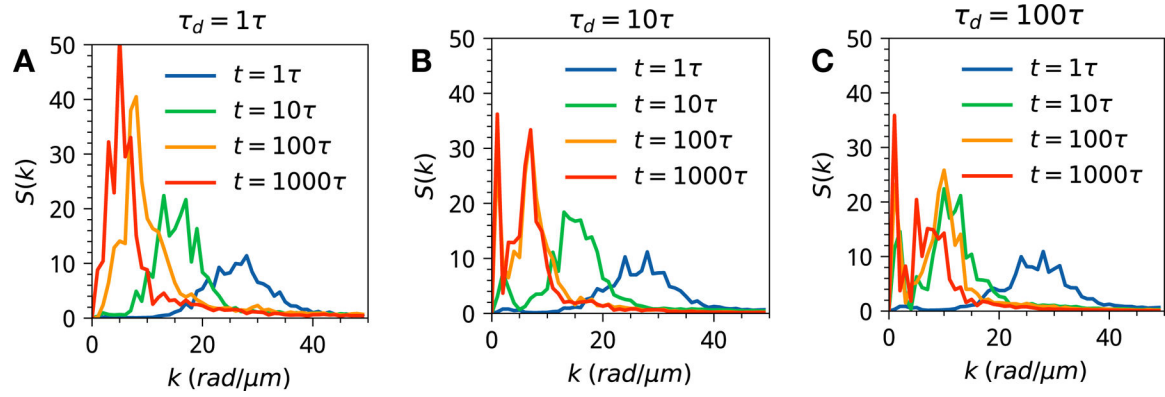


Figure 6.

The dynamic structure factors for the three representative kinetic regimes with significant time-scale disparity between transcription and translation $\tau_P = 100 \tau_R$ (see supporting information for all the results). The inset shows the scaling and power law exponent. The three panels stand for three dynamical regimes: (A) $\tau_d = \tau$ (B) $\tau_d = 10 \tau$ (C) $\tau_d = 100 \tau$.

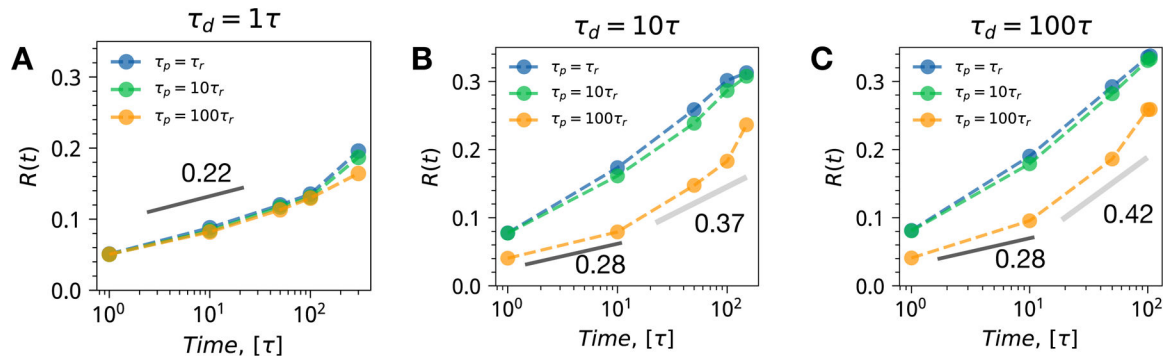


Figure 7.

The dominant length-scale patterns for the three representative kinetic regimes. Each panel shows a combination of transcription and translation time-scales sorted with an increasing time-scale disparity from blue to green to orange. (A) $\tau_d = \tau$ (B) $\tau_d = 10\tau$ (C) $\tau_d = 100\tau$.